Bio-Design and Manufacturing (2025) 8:375–390
https://doi.org/10.1631/bdm.2400212

RESEARCH ARTICLE

An automated raw tissue precision slicing system for methodological advances in biomedical applications: streamlining decellularization in porcine cornea-derived tissue-specific bioink fabrication and beyond

Won Bin Choi[1] · Yeon-ju Lee[2] · Ju Young Park[2,4] · Jinah Jang[1,2,3,4] · Wan Kyun Chung[1]

Received: 28 May 2024 / Accepted: 21 September 2024

Abstract

A decellularized extracellular matrix (dECM) constitutes a pivotal biomaterial created by decellularizing the natural extracellular matrix (ECM). This material serves as a supportive medium for intricate cellular interactions, fostering cell growth, differentiation, and organization. However, challenges persist in decellularization, necessitating a balance between preserving the ECM structural integrity and achieving effective cellular removal. An approach to enhancing decellularization involves pre-eliminating unnecessary tissues and effectively reducing final DNA levels to lower than 50 ng/mg ECM on preprocessed tissues. Although this strategic step augments decellularization efficiency, the current manual execution method depends on the operator's skill. To address this limitation, this study proposed an automated raw tissue slicing system that does not require tissue preparation for slicing. Through carefully controlled tissue applanation pressure and oscillatory incisions with optimized parameters, the system achieved a precision within ±10 μm in obtaining submillimeter-scale tissue slices of the porcine cornea while avoiding significant microscopic complications in the tissue structure, as observed by tissue histology. These findings suggested the system's capability to streamline and automate preliminary tissue slicing operations. The efficacy of this approach for decellularization was validated by processing porcine corneas using the proposed system and subsequently decellularizing the processed tissues. DNA level analysis revealed that sliced, subdivided tissues created by this system could expedite DNA reduction even at the initial steps of decellularization, enhancing the overall decellularization procedure.

✉ Jinah Jang
jinahjang@postech.ac.kr

[1] Department of Mechanical Engineering, Pohang University of Science and Technology, Pohang 37673, Republic of Korea

[2] BioBricks Co., Ltd., Pohang 37673, Republic of Korea

[3] School of Interdisciplinary Bioscience and Bioengineering, Pohang University of Science and Technology, Pohang 37673, Republic of Korea

[4] Department of Convergence IT Engineering, Pohang University of Science and Technology, Pohang 37673, Republic of Korea

Graphical abstract

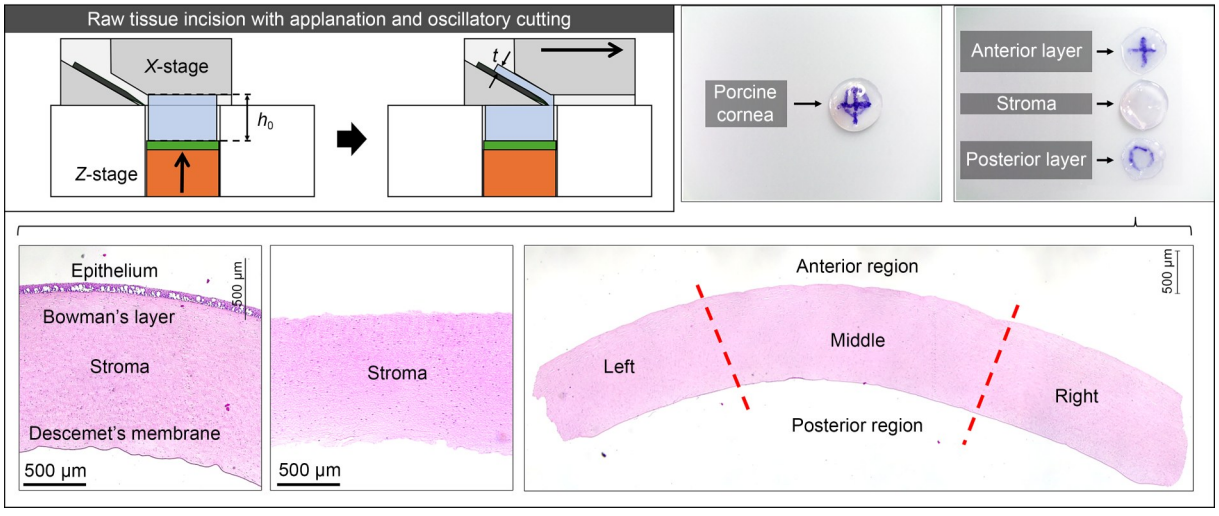

Keywords Raw tissue slicing · Submillimeter-scale slices · High-precision · Oscillatory incision · Applanation · Decellularization

1 Introduction

Tissue engineering has made significant advancements in addressing diverse biological and medical challenges. Among its primary areas of focus is restoring and replacing damaged tissues and organs. The pivotal component enabling these objectives is biomaterials, which assume a central role in this field [1–4]. The importance lies in developing microstructures capable of replicating structural functionalities of the native extracellular matrix (ECM). This capability enables preserving the distinctive spatial distribution of structural and functional components, providing an environment for intricate cellular reactions and assisting cell growth, differentiation, and organization [4–9]. A noteworthy biomaterial in this context is decellularized ECM (dECM), known for its ability to preserve the natural ECM's functional and structural proteins, encompassing various types [10–13]. dECM utilization in tissue engineering has shown effectiveness across various applications, enabling the significant restoration of tissue homeostasis and promotion of the regeneration process [1, 10, 11, 14–21].

For instance, when a porcine cornea is decellularized, its dECM can be a key ingredient in various medical applications, particularly in fabricating tissue-specific bioinks [21–24]. Using xenogeneic tissues, which are not limited to porcine corneas, offers significant advantages, especially in eliminating the need to find a donor. However, allogeneic and xenogeneic tissues and cell-derived ECM carry risks of interacting with the recipient's body, triggering a host-reactive response and causing detrimental effects that hinder in vivo applications [25, 26]. Such effects include inflammation, foreign-body rejection, and immune reactions, all attributed to the presence of cells or cell-derived materials within the ECM [27]. To mitigate these risks and repopulate new cells, tissue and organ decellularization is imperative to manufacture ECM-derived materials [26, 27].

It is difficult to determine that the status of a target tissue is decellularized because the definition is not strictly defined by quantitative metrics. However, various guidelines have been established based on studies in which an in vivo constructive remodeling response was observed and adverse cell and host responses were avoided [26, 28, 29]. The two main quantitative criteria for the sample tissue are: (1) less than 50 ng double-stranded DNA (dsDNA) per milligram of dry weight and (2) less than 200 basepair (bp) DNA fragment length [10, 13, 28–30].

Diverse decellularization techniques, including enzymatic, chemical, and physical methods, have been developed and refined over time to efficiently remove cellular components from various tissues [10, 26, 31–33]. However, a fundamental challenge lies in finding a delicate balance between preserving the ECM structural integrity and achieving effective decellularization. Strong decellularization approaches may result in significant ECM disruption or tissue damage [34–37]. Meanwhile, methods aimed to preserve the ECM structural integrity and alleviate the influence of the reaction could leave residual cellular debris and might be insufficient on their own to achieve the high degree of cell removal necessary to prevent cell and host responses [10, 21, 38–41]. This inherent trade-off highlights the ongoing need for research and innovation to optimize decellularization processes, ensuring that the tissue and

ECM retain their essential properties while becoming suitable for diverse biomedical applications.

To enhance and optimize the decellularization performance, a strategic approach for removing unnecessary tissues can be conducted before decellularization [21]. For instance, this approach has been applied in porcine corneas, where cells were pre-eliminated by manually removing thin tissue layers from top and bottom corneal tissues using a surgical blade, retaining only the stroma. By performing this preliminary tissue removal procedure on a porcine cornea before decellularization, a favorable decellularization outcome can be achieved, resulting in DNA levels of lower than 50 ng/mg. This ensures the attainment of these desired decellularization criteria by eliminating cell layers from the tissue sample. In contrast, decellularization of porcine corneas without this preprocessing step often results in DNA decellularization exceeding the acceptable limit. This manual cell removal method requires precise blade control, introduces variability in the quality of pre-decellularization, and prolongs the operation time, thereby making the process highly dependent on the operator's skill level. Therefore, an automated approach for consistent cell removal can eliminate the need for operator involvement.

Automated tissue slicing systems equipped with specially designed blade systems capable of controlling incision parameters have demonstrated the ability to achieve submillimeter-scale tissue slices [42–45]. However, their limitations restrict their application to specific tissue types, such as soft delicate tissues (e.g., the brain and liver). Consequently, these systems are not optimized for fibrous organs or connective tissues (e.g., corneal stroma, skin, and airway mucosa) with robust mechanical properties [42–45]. Systems that can generate thin tissue slices still necessitate tissue fixation methods (e.g., paraffin wax), adding additional steps to the overall process. Expanding the tissue types sliced by an automated system could facilitate broader applications of decellularization process optimization through preprocessing. Current constraints emphasize the necessity for a solution that accommodates distinct mechanical properties exhibited by fibrous organs and connective tissues while ensuring a consistent and effective incision process without needing preprocessing, promoting simplicity and efficiency.

This study developed a coordinated delamination instrument using applanation and cutting (CoDIAC) to validate the use of applanation and oscillatory incision techniques for obtaining precise thin tissue slices of raw porcine corneal tissues. The CoDIAC system employs applanation to securely hold the tissue sample in place and utilizes controlled oscillation to enable precise and effective incisions. By applying carefully controlled pressure to the tissue sample, uniform flattening and fixation of the tissue are achieved. With optimized parameters for oscillatory incisions, this technique can effectively cut through fibrous tissues without requiring preprocessing while maintaining uniform submillimeter-scale tissue slices. This study verified the slicing performance of CoDIAC by conducting cell pre-elimination slicing experiments on cadaveric porcine eyes, specifically targeting corneal tissues composed of fibrous collagen [46]. In the following stages of the investigation, quantitative analysis was conducted on the processed cornea, followed by tissue histology, to meticulously examine the microscopic influence of the system. This investigation yielded valuable insights, as tissue histology examination allowed for the inspection of ECM structural integrity and potential microscale complications. The efficacy of the proposed system in the decellularization process was demonstrated by decellularizing corneal tissues processed by CoDIAC. DNA level analysis was performed after each significant decellularization step, indicating the system's effectiveness in the decellularization process.

Results demonstrated that the core principles employed in corneal tissue slicing by the proposed system effectively enable controlled incisions in fibrous connective tissues of raw porcine corneas. Furthermore, the observed rapid decrease in DNA levels in the processed tissue slices after decellularization suggests potential improvements in efficiency, productivity, and consistency, leading to the potential of streamlining the decellularization process.

2 Methods

2.1 Development of a precise tissue slicing system enhanced by applanation and oscillatory incision techniques

The CoDIAC system, an automated tissue slicing tool, was developed to produce submillimeter-scale slices from tissues or organs. It comprises two primary components: an incision module and a vertical stage (Fig. 1). The incision module, equipped with a direct current motor (PGM22-2238-DH; Motor Bank, Seoul, Republic of Korea) linked to a cam mechanism, delivers oscillatory incisions with an adjustable frequency of up to 12 Hz. The blade oscillation frequency can be controlled by the input voltage of the motor. With the replacement of the cam, the system can further modulate the frequency to four times the base value, offering an additional capability for customized slicing. The current model achieves an oscillation amplitude of up to 15 mm, which can be modified based on the cam size. The vertical stage applies controlled pressure up to 2.8 MPa on the tissue, which is driven by a servo motor (XM430-W210-T; ROBOTIS, Seoul, Republic of Korea) and regulated via a pressure sensor (QA6P; Marvel Dex, Seongnam, Republic of Korea). Each module operates on separate axes, with the incision module moving along the *X*-axis and the vertical

stage along the *Z*-axis (Fig. 1b). The incision module length was controlled by a linear actuator (12Lf-10PT-40; IR Robot, Bucheon, Republic of Korea), which offers a maximum speed of 116 mm/s over a 40-mm range and maintains a 9.75-μm resolution with an accuracy of ±30 μm or better. CoDIAC ensures automated, consistent tissue slicing under controlled conditions, significantly reducing variability in the slicing process. Table 1 shows the comprehensive specifications of the CoDIAC system.

2.2 Experiment design

2.2.1 Shape standardization of the sample tissue

The porcine cornea was preprocessed by extracting the cornea from the central part of a cadaveric porcine eye with an 8-mm biopsy punch. This procedure standardized the target tissue's form into a cylindrical configuration with variable heights. Consequently, uniform cylindrical tissue specimens, namely "cornea tabs," exhibited a consistent diameter but diverse heights. The approximate height of the cornea tab, representing the central thickness of the porcine cornea, can vary in thickness [47]. Therefore, an adaptive incision method must accommodate this delicate scale while meeting precise accuracy standards.

2.2.2 Experiment setup

Cadaveric porcine eyes were used for the performance validation of the proposed systems. The porcine eyes were deep-frozen (−80 °C) within 6 h of enucleation to preserve the samples. Before the experiment, the eyes were thawed by placing them in a 4 °C chiller for 12 h. Surgical scissors were subsequently used to remove any residual tissues around the eye that had not been removed by the supplier. An 8-mm biopsy punch was utilized to extract a circular

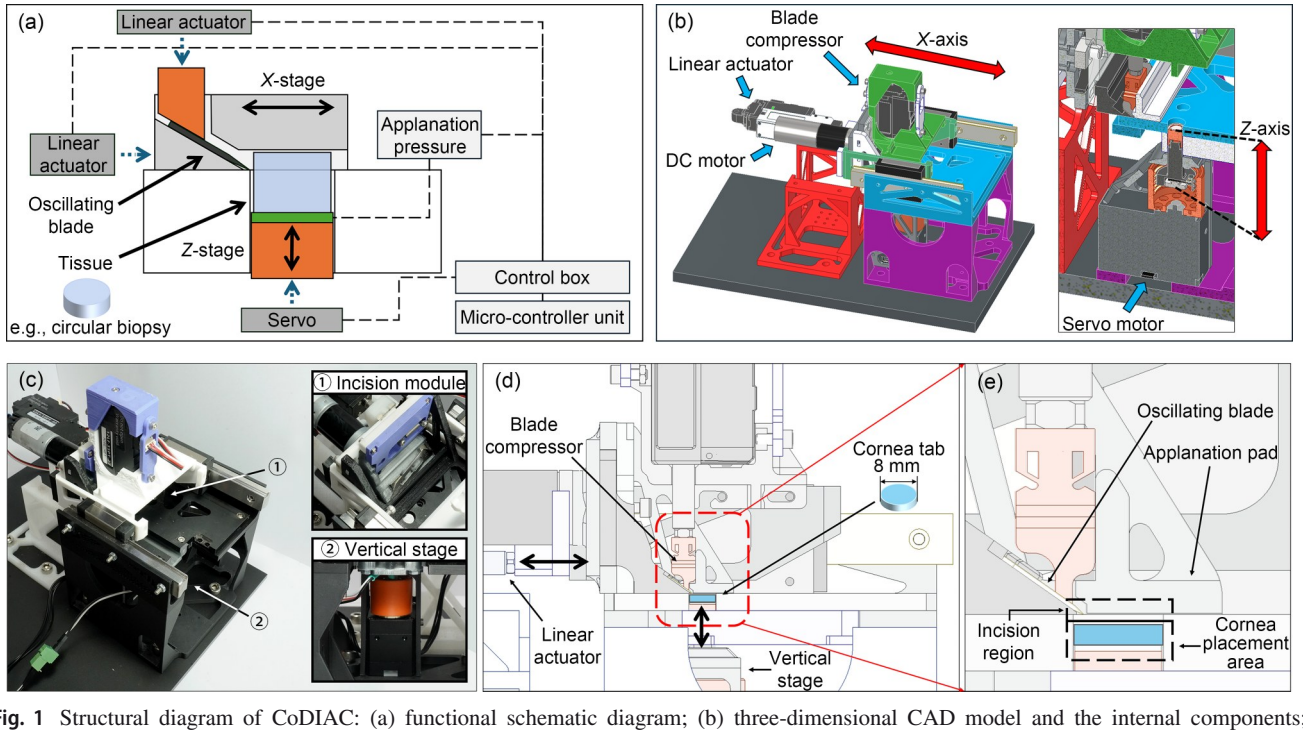

Fig. 1 Structural diagram of CoDIAC: (a) functional schematic diagram; (b) three-dimensional CAD model and the internal components; (c) main function modules of the CoDIAC system; (d) cross-sectional image of the system mechanism; (e) close-up view of the applanation incision mechanism. CAD: computer-aided design; DC: direct current

Table 1 Detailed specifications of CoDIAC

Component	Drive							Oscillation		
	Max. speed (mm/s)	Distance (mm)	Resolution (μm)	Accuracy (μm)	Max. pressure (MPa)	Motor	Encoder	Max. blade speed (mm/s)	Max. frequency (Hz)	Max. amplitude (mm)
Incision module	116	40	9.75	±30	–	Coreless DC linear motor	10 kΩ linear potentiometer	180	12	15
Vertical stage	3.2	14	0.5	±2.0	2.8	Coreless DC motor	Contactless absolute encoder	–	–	–

tissue sample (referred to as a cornea tab) from the eye. Subsequently, the sample was meticulously rinsed in phosphate-buffered saline and promptly sliced after a thorough washing process. The entire experiment procedure was recorded for each trial using a digital single lens reflex (DSLR) camera (ICLE-7ME; Sony, Tokyo, Japan), including the time data.

2.2.3 Experiment procedure

During the incision of the given porcine cornea tab, the system underwent four stages of operation: engagement, calibration, incision, and disengagement. In the engagement phase, the cornea was placed in the cornea placement area and the incision module covered the cornea. The applanation pressure was calibrated once the cornea tab was overlaid with the applanation pad. At this point, the cornea was elevated to the applanation pad in the vertical direction, during which the pressure was gradually increased until the ideal applanation pressure was achieved. Next, the incision began by operating the oscillating blade and driving the blade at a constant speed. After a complete coverage of the cornea tab area by the blade, the disengagement process involved halting the blade's motion, retracting the oscillating blade, and lowering the processed cornea tab away from the incision region.

The proposed device applied two distinct tissue slicing methods to porcine cornea tabs. First, consecutive tissue slices were generated through repetitive system operation after the cornea was inserted. This process resulted in multiple slices on the same cornea tab. Second, layer-specific tissue sections were created to selectively remove the anterior (epithelium+Bowman's layer (BL)) and posterior (endothelium+Descemet's membrane (DM)) corneal layers from the cornea tab, separating those layers from the stroma. This involved removing one tissue layer initially and subsequently flipping the cornea tab to address the other tissue layer. The order of anterior and posterior corneal layer removal was randomized.

2.2.4 Measurement and analysis

To interpret the outcomes of the proposed system, a range of metrics were measured and analyzed, including a postoperative analysis.

(1) Thickness: The cornea tab thickness was measured for the entire cornea, consecutive slices, removed anterior and posterior corneal layers, and the stroma. Using a micrometer (293-234-30; Mitutoyo Corporation, Kawasaki, Japan), the thickness of each sample was acquired with an accuracy of ±1 μm, a resolution of 1 μm, and an error range within ±0.3 μm, resulting in a potential reading error of ±1.7 μm (0.68% margin of error). For precise results, measurements were taken just before tissue deformation by detecting contact between the corneal tissue and the spindle face using a transistor-amplified capacitive touch circuit attached to the spindle faces (a detailed description is provided in the supplementary information). When the spindle face touched the corneal tissue, the light-emitting diode illuminated; therefore, the thickness of the tissue was measured just before deformation. The complete thickness was measured before the incision, and the thickness of the sliced tissue layers was measured immediately after the incision.

(2) Mass: Immediately after the incision, consecutive slices and three tissue layers (stroma, anterior, and posterior corneal layers) were measured with an analytical balance (BCE224i-1s; Sartorius, Göttingen, Germany). The total mass was determined by summing the masses of each individual layer rather than being measured independently. Before being placed on the analytical balance, external fluid was removed from all tissue samples by gently tapping them with a nonwoven fabric wipe (KM WW-2209; Ansung, Republic of Korea) to absorb the fluid.

(3) Applanation pressure: During incision, the pressure exerted on the cornea using the vertical stage on the applanation pad was recorded via real-time logging. This record was supplemented with data on applanation pressure, time, and blade drive distance. Consequently, users could correlate pressure values at specific time points and blade drive distances.

(4) Operation time: Based on the video showing the entire operation of the proposed system, the time required in each step was analyzed for all trials. The start time was set when the cornea tab was positioned onto the designated cornea placement area, whereas the end time was defined as the moment the cornea was released from the system and lifted clear from the incision site. The operation time in the engagement phase was measured from the start time until the applanation pad fully encompassed the cornea. The calibration phase was recorded until the oscillating blade was activated. Subsequently, the incision phase was tracked until the oscillating blade stopped. The disengagement phase was quantified during the retraction of the blade until the end of the operation.

(5) Tissue histology: Two types of staining were utilized to observe layer removal at the microscopic level. For tissue histology analysis, hematoxylin and eosin (H&E) staining and 4',6-diamidino-2-phenylindole (DAPI) staining were utilized to observe the outcome of delaminated tissues. H&E staining enabled us to observe the overall characteristics of the incision site and assess the successful removal of cell layers (epithelium, BL, DM, and endothelium) by the system. In addition to H&E, DAPI staining was concurrently conducted to further examine the presence of DNA. Whereas intralayer cells were present within the stroma, the DAPI-stained tissue histology image helped determine the presence

of high-density cell layers on the processed cornea.

(6) Decellularized tissue dsDNA measurement: After the sample tissues were delaminated using the proposed device, they underwent a decellularization process involving purification (5 mg/0.2 μL). During the purification task, after each detailed step, portions of the samples were freeze-dried and subjected to DNA digestion, ensuring an accurate quantification of the DNA content in decellularized samples. DNA quantification utilized the DNA PicoGreen assay, which employed fluorescence intensity to precisely determine the amount of dsDNA within the samples. For the decellularization task and dsDNA assays, the GeneJET genomic DNA purification kit (K0722; Thermo Fisher Scientific, Waltham, MA, USA) and the PicoGreen kit (Quant-iT^{TM} PicoGreen^{TM} dsDNA assay kits and reagents) were used, respectively.

The solution containing the dECM obtained from decellularization underwent dilution, resulting in a dECM concentration of 2.5 mg/mL (C_{dECM}), which served as a correction factor. Using this correction factor, the dsDNA concentration (C_{DNA}) obtained from the PicoGreen assay allowed us to determine the amount of DNA per 1 mg dECM (M= C_{DNA}/C_{dECM}).

Sample tissues processed by the proposed device were categorized into two groups for investigation. In the first group, layer-specific incisions (anterior and posterior corneal layers) were made to obtain the whole stroma. In the second group, consecutive incisions were made on a single piece of corneal tissue, resulting in a subdivided stroma. In both scenarios, anterior and posterior corneal layers were removed before decellularization. To summarize, layer-specific incisions yielded a whole cornea, whereas consecutive incisions resulted in a subdivided stroma. Both were decellularized, and DNA levels were observed for each group. This systematic comparison aimed to assess the efficacy of the proposed system in the decellularization process.

3 Results and discussion

3.1 Design and system parameters of CoDIAC

A microkeratome can offer potential advantages for corneal tissue incisions; however, due to its intended use in short-duration surgical procedures, there are limitations in integrating a microkeratome into the system. Therefore, key incision parameters have been referred to and implemented in the automated system. Slicing is driven by the stress exerted by the blade. This includes shear stress resulting from the blade's motion, where the blade speed is one of the pivotal parameters that influence this shear stress [48]. For stable long-term operation, a low-speed actuator (planetary gear direct current motor; rated speed: 398 r/min, rated torque: 791 gf-cm; 1 gf-cm=9.806 65×10^{-5} N·m) was used instead of a high-speed variant commonly found in microkeratomes. To replicate the oscillation speed of the microkeratome blade with this setup, the frequency was lowered, and the amplitude of the oscillating blade was increased. The frequency was chosen based on the motor's capability for long-term use and the operational duty cycle. The amplitude was calculated using the following formula:

$$A_O = f_O/(f_M \times A_M),$$

where A_O represents the oscillation amplitude, f_O represents the oscillation frequency, f_M represents the microkeratome frequency, and A_M represents the microkeratome amplitude. Therefore, the parameters were modified to a frequency of 6 Hz and an amplitude of 9.5 mm, yielding a blade speed of 57 mm/s. This adjustment was based on the instrument settings of the Carriazo-Pendular microkeratome (Schwind Eye-Tech Solutions GmbH & Co., Kleinostheim, Germany), which typically exhibit oscillation frequencies from 150 to 250 Hz [49].

The current system was developed to validate the concept of utilizing applanation and oscillatory slicing to achieve effective and precise incisions in raw tissues. Consequently, scalability is another crucial aspect of this research that needs further investigation. Researchers can contemplate the potential scalability of the system by examining its primary parameters. One of the primary parameters controlled in this system is the blade speed, which remains unaffected by the slice area and is solely influenced by the oscillation frequency and amplitude. Although an increased area could indeed influence the applanation pressure, a critical determinant in the slicing outcome of the raw tissue, the vertical stage equipped with a pressure sensor can compensate for such variations. This can be achieved by adjusting the applanation force, effectively compensating for any increase in area. Naturally, if the area is expanded, the vertical stage with the pressure sensor must be redesigned to accommodate the larger area.

To ensure stable and coordinated oscillatory motion of the blade during tissue incision, an incision module was designed. The module consists of two major design features: a cam mechanism and an oscillating blade. The cam mechanism linearly oscillates the oscillating blade with a frequency of 6 Hz and an amplitude of 9.5 mm, which can be driven into the tissue to achieve incision (Fig. 2a). However, the thickness of the surgical blade (Feather No. 25; thickness: 400 μm) could compress surrounding tissues, generating pressure and shear stress on the tissue plane during incision due to its increased contact area, which might impact the incision performance (Fig. 2b). To mitigate this phenomenon, the surgical blade was installed on the oscillating blade at an inclination of 35° relative to the incision plane, in accordance with the angle reference employed in conventional

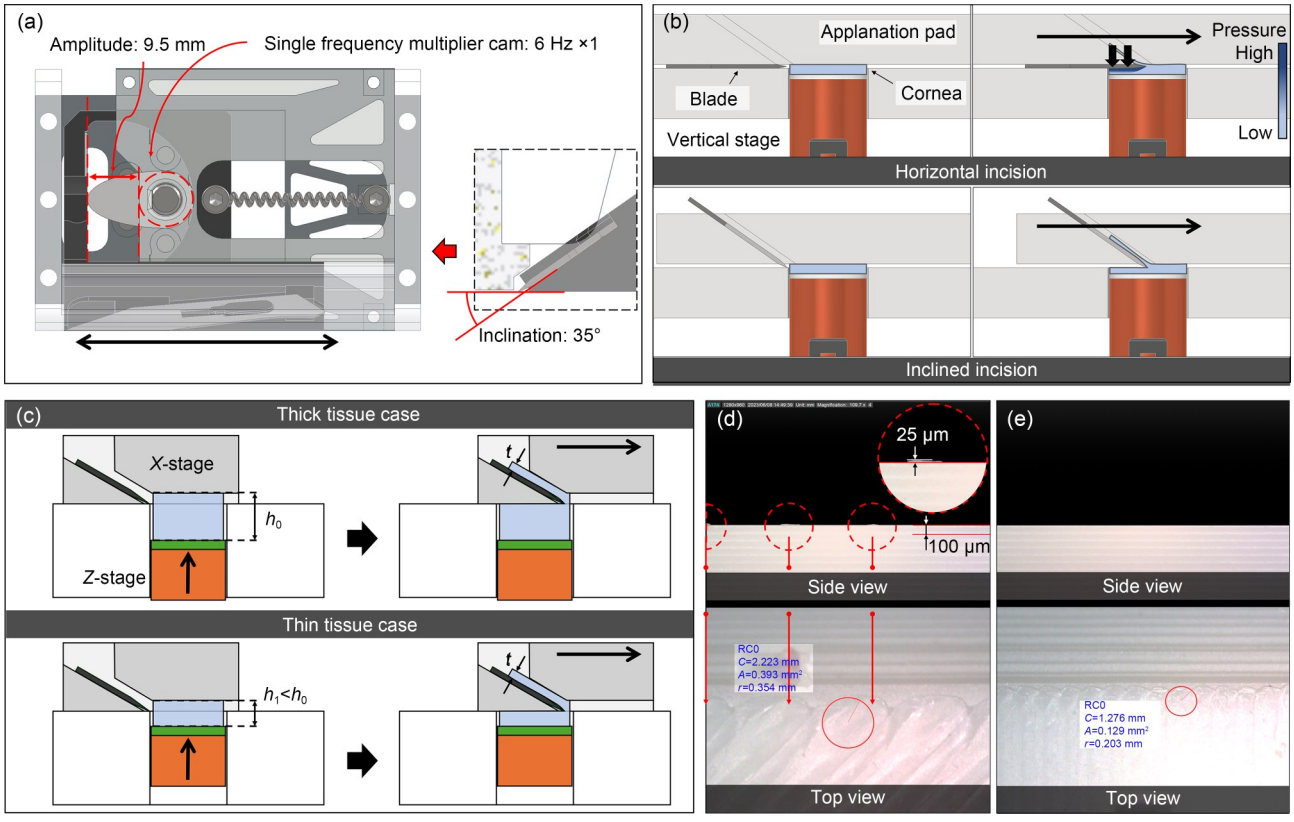

Fig. 2 Critical design aspects in the incision module. (a) Incision module design and major parameters. (b) Difference between the horizontal and inclined incisions. The inclined incision can lessen the effect of blade thickness on corneal tissue samples. (c) An adaptive incision approach to accommodate the variation in tissue thickness. (d) Bumps observed on the applanation pad can lead to complications in incision performance. (e) Bumps were eliminated from the applanation pad after postprocessing, ensuring a smooth surface

microkeratomes (Fig. 2a) [49]. The blade was secured with magnets and a blade compressor to ensure stability.

The height of the cornea tabs varies among the porcine eye samples. Therefore, a passive adaptation method that can accommodate this variation is necessary to achieve a constant incision height. The applanation pad was affixed onto the incision module, ensuring a constant distance between the applanation plane and the oscillating blade's incision plane, keeping the incision height constant regardless of the cornea tab (Fig. 2c). Therefore, users can control the tissue slice thickness by controlling the gap distance between the blade and the applanation pad. The gap distance can be modified by changing the applanation pad installed on the oscillating blade (Fig. S2 in the supplementary information). When the oscillating blade is activated, the cornea tab can be compressed onto the applanation plane, and the incision module can slide over the cornea tab, removing a tissue layer identical to the specified incision height.

The optimal thickness of tissue slices varies with the application. In this study, the thickness was set to 250 μm, which is a large margin to ensure the removal of cell layers within the corneal tissue. The current system has limitations regarding the usability of slice thickness modification. Slice thickness can be controlled by adjusting the gap distance between the blade and the applanation pad. However, this process requires removal and installation, requiring users to follow multiple operation steps. Therefore, introducing a variable gap distance control mechanism integrated into the system could streamline the process of setting the slice thickness, enhancing the usability and efficiency of the system.

The cornea tab was compressed in a coordinated manner by a vertical stage equipped with a pressure measurement function. Compression pressure regulation was achieved using a proportional-integral-derivative (PID) closed-loop controller. The tissue should remain within the designated cornea placement area and incision region to facilitate seamless operation of the incision module. Therefore, a displacement guard surrounding the vertical stage was installed to inhibit any movement of the cornea tab.

The surface roughness of the applanation pad plays a critical role in ensuring a successful incision in the raw tissue. If the pad exhibits surface defects that hinder the achievement of the required smoothness, these defects may result in tissue pulling and displacement, leading to incision failure. Moreover, the tissue could be stuck within the incision module due to unexpected tissue relocation. Considering this issue, the applanation pad fabricated using

fused deposition modeling underwent postprocessing to ensure a smooth surface and eliminate all surface imperfections (Figs. 2d and 2e). Smoothness should be achieved such that when the applanation pad compresses the corneal tissue with a 2-kg load, the tissue should be able to slide freely without resistance under the applanation pad.

Preventing contamination when operating and maintaining the device is essential. To facilitate the sterilization process, components that directly contact the tissues are designed for easy detachment, utilizing magnetic connections for swift assembly and disassembly from the system. The blade used in the system is sterile, as it undergoes sterilization during the manufacturing process and is sealed in airtight packaging until it is opened for use [50]. After tissue cutting, the blade can be readily removed and replaced, facilitated by its secure fixation using magnets.

3.2 Submillimeter-scale raw tissue incision and delamination through CoDIAC

Multiple porcine corneal tissue samples were used to evaluate the performance of incisions made with the proposed device. Four consecutive incisions were made on a single piece of corneal tissue for 10 porcine eyes. For the layer-specific case, 10 porcine eyes were used, and anterior and posterior corneal layers were removed from the cornea; thus, two incisions were made on a single sample. To mitigate the potential impacts of the incision sequence, the order of incisions was altered for each trial.

After consecutive incisions, a single cornea tab was separated into five tissue slices due to the four incisions. The final tissue slice was neglected because it was not sliced in a controlled manner using the proposed system but was a residue of the delamination process. Therefore, using 10 porcine eyes, a total of 40 slices were produced, with thicknesses measuring (252±8) μm. When sliced using the layer-specific method, a single porcine cornea sample can be separated into three parts: stroma, anterior (epithelium and BL) corneal layer, and posterior (endothelium and DM) corneal layer. Anterior and posterior corneal layers were removed at thicknesses of (252±7) μm and (251±6) μm, respectively, leaving the stroma at a thickness of (757±48) μm (Fig. 3 and Table 2). The target thickness of the sliced tissue

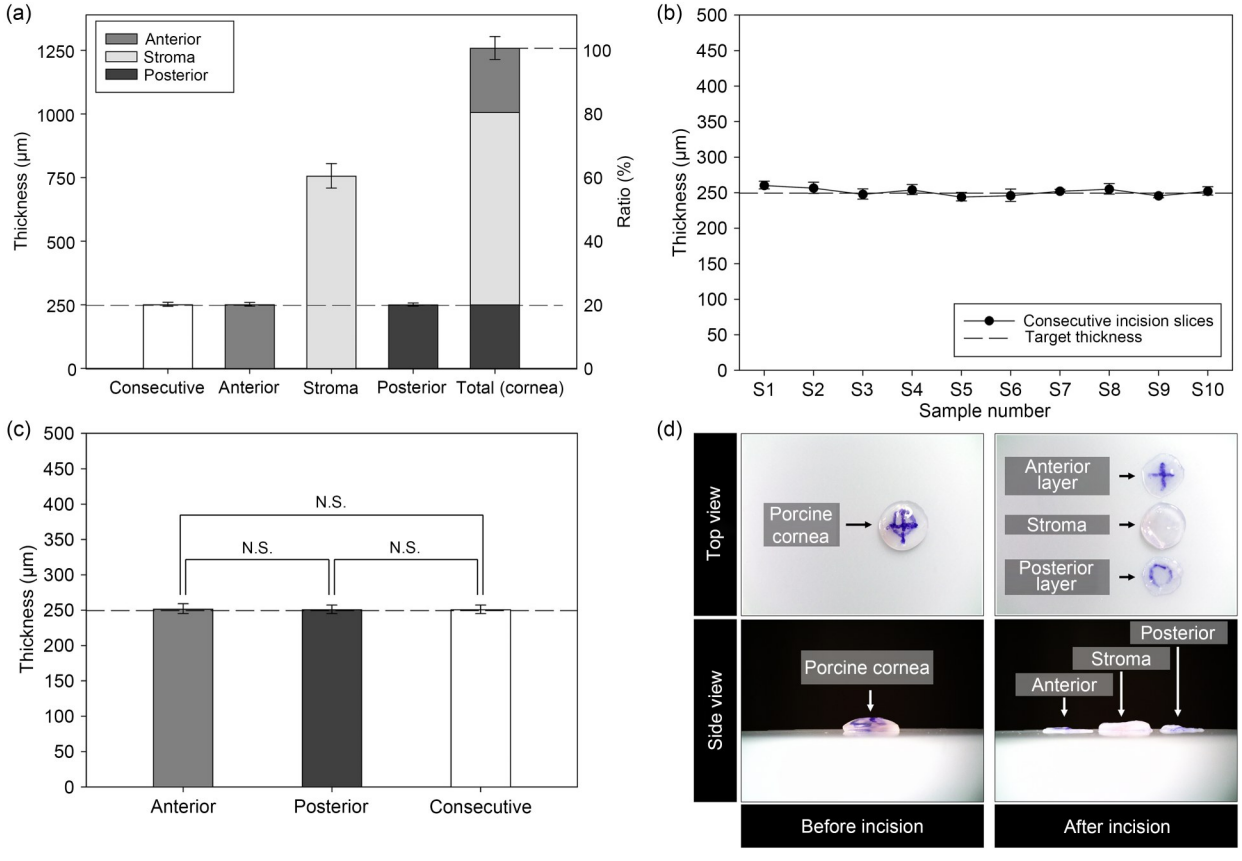

Fig. 3 Raw tissue incision thickness evaluation and analysis. (a) Slice thickness and ratio of the porcine cornea in consecutive incision case (n=40) and layer-specific incision case (n=10) divided into stroma, anterior corneal layer (epithelium and BL), and posterior corneal layer (endothelium and DM). (b) Layer thickness according to the sample number (order) of the tissue samples undergoing consecutive incision (n=40). (c) Statistical significance analysis of the sliced layer thickness (n=10 for each layer and n=40 for consecutive slices). (d) Porcine cornea sample separated into three parts by raw tissue incision using the proposed device. Data are expressed as mean±standard deviation (N.S.: not significant)

Table 2 Thickness of each layer acquired by the system using CoDIAC

Incision case		Thickness (μm)		Ratio (%)	Error (μm)	Size
		Average	Standard deviation			
Consecutive	Slices	252	8	–	2	40
	Total (cornea)	1239	33	–	–	10
Layer-specific	Stroma	757	48	60.1±1.0	–	10
	Anterior	252	7	20.0±0.9	2	10
	Posterior	251	6	20.0±0.9	1	10
	Total (cornea)	1259	45	–	–	10
	Total (slices)	251	6	–	1	20

Error=|target thickness – average thickness|, with target thickness being 250 μm. In the layer-specific incision case, the corneal tissue is separated into three layers: stroma, anterior corneal layer (epithelium and BL), and posterior corneal layer (endothelium and DM). The red indicates the tissue slices

using the proposed system was set to 250 μm, with observed slices achieving the target thickness with 2.4% variation from the mean (within ±10 μm).

Given these results, the proposed system can achieve submillimeter-scale raw tissue incisions using applanation and an oscillating blade. The target layer removal thickness of 250 μm is large considering the actual thickness of the epithelium, BL, DM, and endothelium [47]. However, the target thickness can be modified by changing the applanation pad installed on the system (Fig. S2 in the supplementary information).

3.3 Tissue removal mass measurement and removal precision

The supplementary experiment assessing the slice mass is a complementary validation of the slice thickness evaluation conducted previously. From the linear relationship between mass and thickness, congruence is expected between the ratio of thickness to mass measurements of the sliced tissue relative to the total tissue sample. By measuring the thickness and mass of tissue slices, this study aimed to ensure the accuracy and reliability of thickness measurements.

Mass measurements were taken of tissues mainly composed of ECM (stroma) and tissues with high cell density levels (anterior and posterior corneal layers) promptly after incision. The masses of the removed anterior corneal layer ((17.3±0.4) μg) and posterior corneal layer ((17.7±0.6) μg) accounted for (20.6±0.5)% and (21.1±0.7)%, respectively, of the entire corneal tissue obtained from an 8-mm biopsy punch (Fig. 4 and Table 3). The anticipated ratio of the removed mass is expected to exhibit a similar value to the thickness, considering the linear relationship between the mass and thickness when a constant area is maintained (Tables 2 and 3).

Given this relationship, the system's ability to create submillimeter-scale thick incisions with microscale precision directly influences the control of the removed mass.

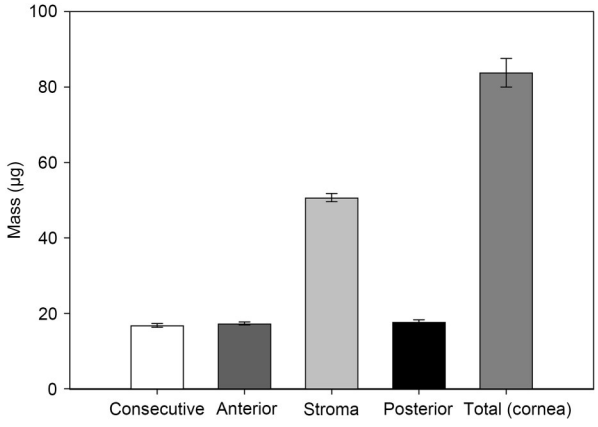

Fig. 4 Acquired mass of the tissue slices in the consecutive incision case (n=40) and layer-specific incision case (n=10) by the proposed system. Data are expressed as mean±standard deviation

This precision ensures a significant reduction in variability, which is typical in manual processes. As a result, this system offers consistently reliable tissue processing that is not dependent on the operator's skill level, which is a critical limitation in manual procedures.

3.4 Optimal applanation pressure range for effective raw tissue incision and fixation

The optimal applanation pressure for raw tissue incision of the porcine cornea was 40–45 kPa. If the pressure drops below the lower limit, premature tearing of the tissue (tissue clipping) may occur, which leaves residual cell layers on the acquired stroma (Fig. 5b). Therefore, a PID controller was utilized to regulate the applanation pressure within the optimal pressure range. The gains of the PID controller were determined using the Ziegler-Nichols method, a heuristic approach for tuning the controller gains [51, 52]. As a result, the clipping phenomenon could be prevented, and a complete clean incision of the raw corneal tissue could be created (Fig. 5c). Furthermore, it is essential to exercise

Table 3 Mass of each layer acquired by the system using CoDIAC

Incision case		Mass (μg)		Ratio (%)	Size
		Average	Standard deviation		
Consecutive	Slices	16.8	0.5	–	40
	Total (cornea)	82.1	2.5	–	10
Layer-specific	Stroma	50.3	2.0	60.0±2.3	10
	Anterior	17.3	0.4	20.6±0.5	10
	Posterior	17.7	0.6	21.1±0.7	10
	Total (cornea)	83.8	3.8	–	10
	Total (slices)	17.5	0.5	–	20

The red indicates the tissue slices

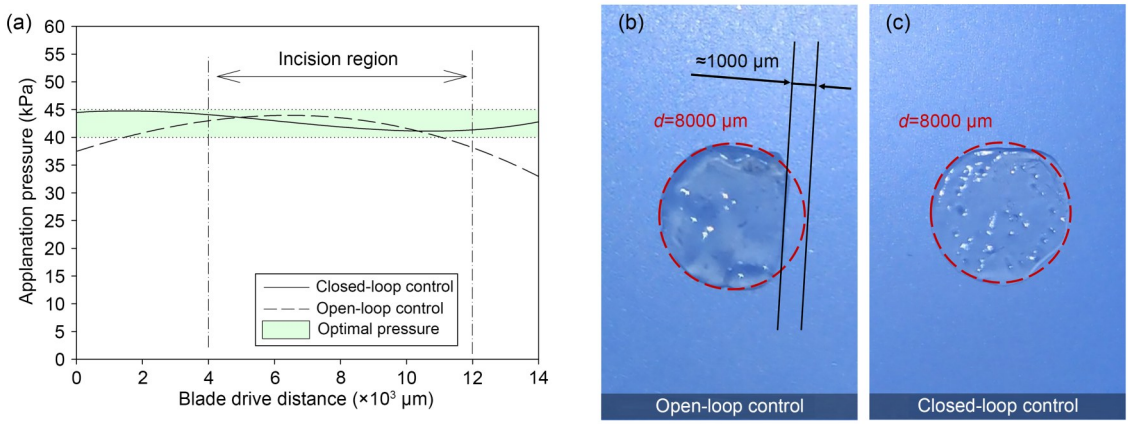

Fig. 5 Significance of applanation pressure control during raw tissue incision. (a) Applanation pressure on the porcine cornea by blade drive distance during incision. A closed-loop PID controller is required to regulate applanation pressure within the optimal range. (b) Premature tissue tearing (tissue clipping) occurred at the anterior/posterior corneal layer due to an applanation pressure drop—1000 μm ahead of the incision termination point. (c) Tissue clipping was prevented by applying a PID controller for optimal applanation pressure regulation

caution against the application of excessive pressure, as this is crucial for preventing potential system failures. This measure also holds significant importance in optimizing the performance of the incision procedure because excessive pressure during tissue applanation can result in heightened friction, generating substantial shear forces on the tissue sample, thus complicating an effective incision.

In short, the optimal pressure for fixing the porcine cornea and achieving submillimeter-scale incisions in the raw tissue was within the range of 40–45 kPa (Fig. 5). Nonetheless, this pressure was established through a series of iterative experiments conducted on porcine corneal tissues. Therefore, the optimal pressure on different tissue types or organisms might differ. In future research endeavors, an analytic model could be established to predict suitable pressure ranges for arbitrary tissues.

3.5 Phase-wise operation time measurement of CoDIAC

The proposed system goes through four tasks to complete the raw tissue incision of the porcine cornea (Fig. 6). First, during the engagement phase, all system components are checked, and the sample tissue placed on the vertical stage is locked into the system ((2.00±0.10) s). Next, in the calibration phase, the vertical stage is controlled to administer the optimal pressure onto the sample tissue ((6.30±0.30) s). After calibration, an incision is made ((5.62±0.27) s), and when the blade reaches the end position, the sample tissue is released, and the system is disengaged ((3.17±0.15) s). In summary, the system requires an operation time of (17.09±0.83) s to execute a single-layer incision of porcine corneal tissues extracted using an 8-mm biopsy punch.

3.6 Cell layer removal efficacy measurement using tissue histology analysis

Although the proposed system can effectively delaminate tissue layers, ensuring the complete removal of cell layers requires further microscopic analysis (Fig. 7). Consequently, all samples were examined using cellular staining methods. By inspection of H&E and DAPI images, the porcine cornea control sample was missing the endothelium layer, but the BL, DM, and epithelium were intact (Figs. 7a (control) and 7b). If the tissue sample undergoes incision by the proposed system, only the stromal membrane is retained, with

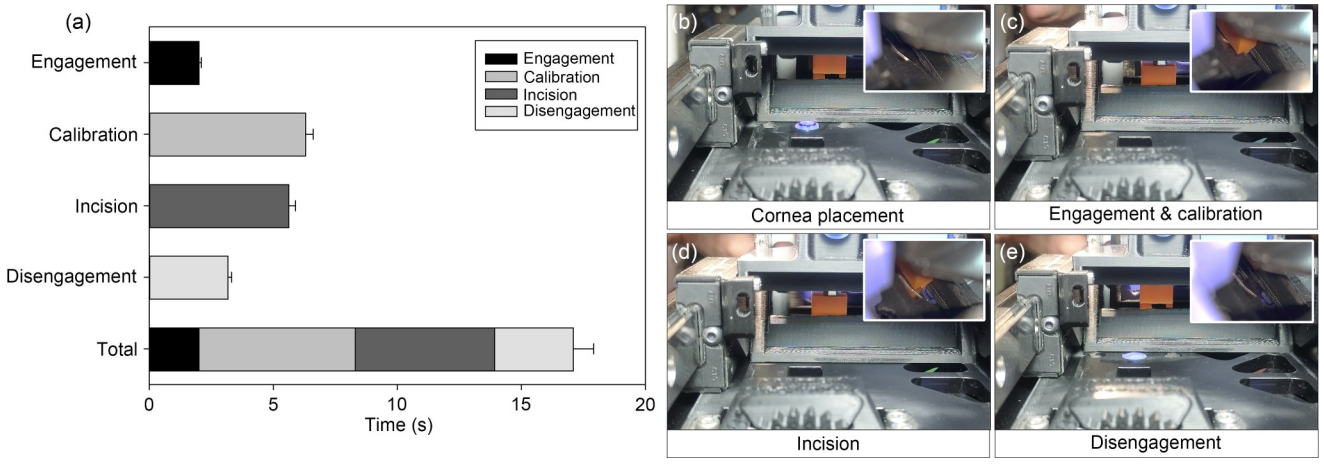

Fig. 6 Process time required for each operational step. (a) Operation time of the proposed device by task type (data are expressed as mean± standard deviation, n=22). The corneal layer incision process includes the following steps: (b) placement of the cornea tab into the cornea placement area, (c) system engagement and calibration of the optimal applanation pressure, (d) incision made by the oscillating blade, and (e) disengagement of the system, stopping the blade and releasing the cornea tab

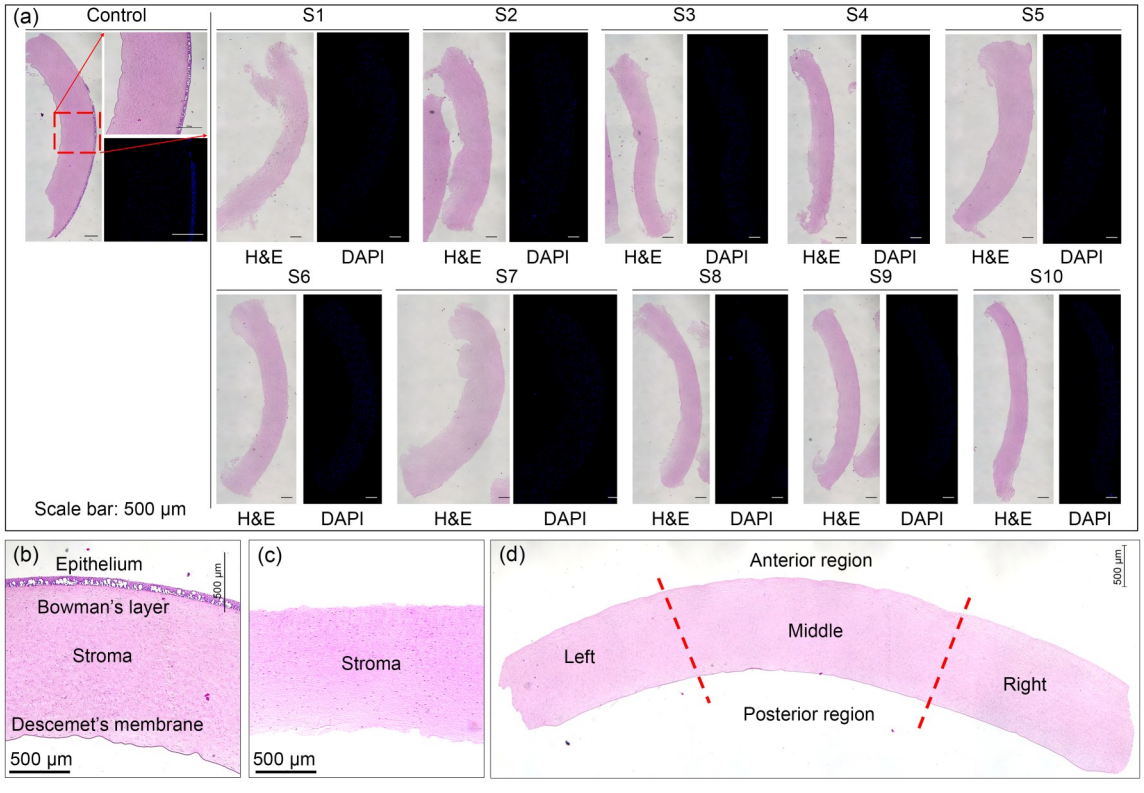

Fig. 7 Microscopy observations of the incision site in the sliced cornea sample. (a) Tissue histology analysis after slicing the sample tissue by two types of staining: H&E and DAPI. The histology slides show the state of the sample tissues after the preprocessing state of removing the cell layers before decellularization. Nuclear remnants may be partially observed in these slides, as they depict tissues in an intermediate stage of decellularization. A control tissue sample involving the extraction of corneal tissue from the porcine eye but without the tissue removal performed by the proposed system was included. H&E and DAPI staining revealed cell nucleus staining, indicating the presence of cells. On inspection, the cell layers (epithelium, BL, DM, and endothelium) were eliminated when processed using the proposed system. (b) Porcine cornea control sample tissue histology image with H&E staining. (c) Cornea sample that underwent layer removal using the proposed system. By observation, the anterior and posterior corneal tissue layers have been physically removed. (d) Evaluation regions of the processed corneal tissue sample to quantify the tissue histology

the epithelium, BL, and DM being completely removed (Figs. 7a (samples) and 7c). The removal of cell layers with high cell density can be inspected by comparing the H&E and DAPI images.

To better understand the system's incision performance, tissue histology was quantified. In the initial step, the "score," representing incision efficacy, was assessed through visual inspection, and its subsequent rating was rated using a predefined rubric. The evaluation process was based on three specific criteria: (1) 2 points for complete incision and removal of anterior and posterior corneal layers, (2) 1 point for partial incision and removal of anterior and posterior corneal layers with some residual regions, and (3) 0 points for failure of incision or that anterior and posterior corneal layers are intact. In the second step, the "cutting rate" was assessed by determining whether the cell layers had been removed from the stroma. The evaluation process involved dividing the sample tissue into multiple regions, and 1 point was assigned if the cell layer was absent.

The cornea sample was divided into three sections (left, middle, and right) for the anterior and posterior regions, resulting in the examination of six sections for each sample (Fig. 7d). This structure allowed for a maximum score of 12 points and a maximum cutting rate of 6 points. In summary, the processed tissue samples exhibited an average score of 11.6 (96.7% of the maximum score of 12) and a cutting rate of 5.7 (95% of the maximum of 6; Tables 4 and 5). All samples demonstrated effective removal of anterior and posterior corneal layers, apart from complications observed in the fifth and seventh samples (S5 and S7).

Table 4 Performance index value "score" for tissue histology quantification

Sample number	Score						Total	Percentile (%)
	Anterior region			Posterior region				
	Left	Middle	Right	Left	Middle	Right		
S1	2	2	2	2	2	2	12	100
S2	2	2	2	2	2	2	12	100
S3	2	2	2	2	2	2	12	100
S4	2	2	2	2	2	2	12	100
S5	0	2	2	2	1	2	9	75.0
S6	2	2	2	2	2	2	12	100
S7	2	2	1	2	2	2	11	91.7
S8	2	2	2	2	2	2	12	100
S9	2	2	2	2	2	2	12	100
S10	2	2	2	2	2	2	12	100
Average	1.8	2	1.9	2	1.9	2	11.6	96.7

Six regions were inspected, and points were assigned based on three quality criteria specified in the evaluation rubric (maximum value for each sample: 12 points)

In Samples S5 and S7, at the edge of the cornea tab, the BL remained attached to the tab, indicating incomplete removal of the cell layer from the stroma. However, the corneal thicknesses in S5 and S7 were greater than those in the other samples. This suggests that the system's ability to achieve stable incisions may be suitable for corneas with a thickness smaller than a certain threshold, beyond which its performance might be compromised.

Table 5 Performance index value "cutting rate" for tissue histology quantification

Sample number	Cutting rate		Total	Percentile (%)
	Anterior region	Posterior region		
S1	3	3	6	100
S2	3	3	6	100
S3	3	3	6	100
S4	3	3	6	100
S5	2	2	4	66.7
S6	3	3	6	100
S7	3	2	5	83.3
S8	3	3	6	100
S9	3	3	6	100
S10	3	3	6	100
Average	2.9	2.8	5.7	95

Six regions were inspected, and points were assigned based on the presence of cell layers (maximum value for each sample: 6 points)

The tissue region where the oscillating blade was used to create the incision had an irregular boundary throughout the entire incision area. Although a surgical blade was in the system, a clean boundary shape was unattainable. This phenomenon could have been influenced by the blade's low oscillation frequency and high motion amplitude, despite its similar oscillating speed to that of the microkeratome. Despite boundary irregularities, the stromal tissue remained structurally intact. This observation suggested that the incision method employed by the proposed system results in minimal disturbance to the ECM architecture and collagen structure. As a result, the risk of potential damage to the basement membrane is likely mitigated.

3.7 Decellularization efficacy assessment of CoDIAC by DNA level analysis

To investigate the effectiveness of the proposed device, DNA level analysis was conducted on the sample tissues (Fig. 8). The analysis involved measuring whole stroma samples (n=10), where anterior and posterior corneal layers were removed using the proposed system. Sliced stroma samples (n=10) were prepared by removing the corneal layers and further slicing the stroma into multiple subdivisions to increase the overall surface area. During decellularization, DNA levels were measured after each major step. The DNA levels in the sliced stroma ((464.19±11.85) ng/mg), which was divided into multiple tissue slices, showed a substantial reduction even during the early stages of the decellularization process, compared to the native stroma ((724.90±5.77) ng/mg). Additionally, the sliced stroma

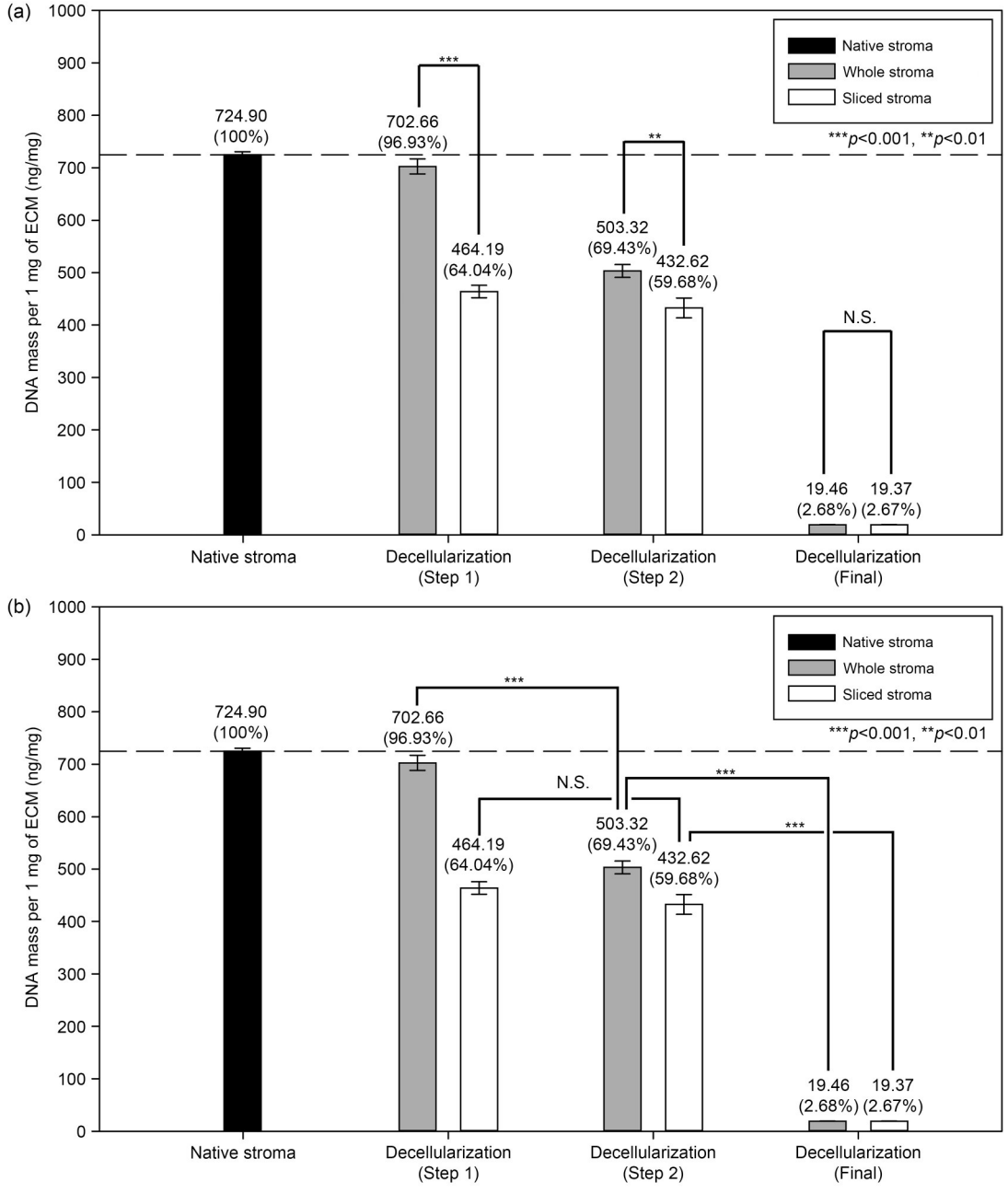

Fig. 8 DNA levels measured within cell layer pre-eliminated cornea samples that underwent decellularization. Statistical significance analysis was conducted between sample types (a) and steps for each process (b). Whole stroma samples (n=10) were obtained by the layer-specific incision method, and subdivided sliced stroma samples (n=10) were obtained by the consecutive incision method. Layer-specific and consecutive slicing methods involve the removal of anterior and posterior corneal layers before decellularization, leaving only the stroma. The purification process for decellularization involves several sequential steps. Compared to the whole stroma samples, the sliced stroma samples demonstrated a faster reduction in DNA levels, even during the early steps of the process. Throughout all steps, DNA levels in the sliced stroma samples remained consistently lower than those in the whole stroma samples with significant differences. Data are expressed as mean±standard deviation ($^{***}p<0.001$, $^{**}p<0.01$)

exhibited significantly lower DNA levels than the whole stroma ((702.66±14.41) ng/mg) at these initial steps. Beyond achieving lower DNA levels at earlier stages, the sliced subdivided stroma consistently exhibited lower variations in DNA levels ($^{***}p<0.001$ and $^{**}p<0.01$) compared to the whole stroma throughout all measured steps. In the sliced stroma case, the DNA level change was insignificant between decellularization Steps 1 and 2.

In summary, results indicated that preprocessing tissues with the proposed system before decellularization can make sample tissues achieve a greater degree of reduction in DNA content, as shown in the sliced stroma case. The insignificant

change observed between the intermediate steps (sliced stroma case; Steps 1 and 2) suggests that certain steps (e.g., Decellularization—Step 2) could be omitted, simplifying the decellularization process. This optimization can reduce the number of steps, associated time, and cost required for the procedure.

4 Conclusions

This study demonstrated an automated method for achieving high-precision submillimeter-scale raw tissue slicing, eliminating the need for preprocessing. By integrating applanation and an oscillatory incision, uniform flattening and fixation of the target tissue were maintained, generating thin slices with a reduced thickness variability within ± 10 μm. As confirmed by tissue histology, the system's incision method ensures minimal disturbance to the ECM architecture and collagen structure, enabling its application in various fields that demand precise submillimeter-scale raw tissue slicing. Stepwise DNA level analysis demonstrated an expedited decrease in DNA levels in the subdivided stroma by the proposed system, even at the initial steps of decellularization, which suggests the system's potential to streamline and reduce the necessary steps in the overall decellularization process. The automated high-precision submillimeter-scale raw tissue slicing system, CoDIAC, can create precise slices in the fibrous tissues of porcine cornea. Although the fundamental operational principle of raw tissue slicing was demonstrated on the porcine cornea, possible expansion in the application of raw tissue slicing to other organs and tissues can be anticipated. The capabilities demonstrated in this study present a promising opportunity for future research to explore methodological advancements in biomedical research.

Supplementary Information The online version contains supplementary material available at https://doi.org/10.1631/bdm.2400212.

Acknowledgements This work was supported by the Alchemist Project 1415180884 (No. 20012378, Development of Meta Soft Organ Module Manufacturing Technology without Immunity Rejection and Module Assembly Robot System) funded by the Ministry of Trade, Industry & Energy (MOTIE, Republic of Korea), and the Technology Development Program (No. S3318933) funded by the Ministry of SMEs and Startups (MSS, Republic of Korea).

Author contributions WBC designed the study, designed and fabricated the coordinated delamination instrument using applanation and cutting (CoDIAC) system, created the control algorithm framework, and conducted and analyzed the tissue incision performance. YJL and JYP performed the tissue histology and DNA level analysis. JJ and WKC supervised the research. All authors revised the final manuscript.

Funding Open access funding enabled and organized by Pohang University of Science and Technology (POSTECH).

Declarations

Conflict of interest JJ is an associate editor for *Bio-Design and Manufacturing* and was not involved in the editorial review or the decision to publish this article. The authors declare that they have no conflict of interest.

Ethical approval This study does not contain any studies with human or animal subjects performed by any of the authors.

Data availability The authors confirmed that all data in this manuscript are original and are available from the corresponding author upon reasonable request.

References

1. Hubbel JA (1995) Biomaterials in tissue engineering. Nat Biotechnol 13(6):565–576. https://doi.org/10.1038/nbt0695-565
2. Koike N, Fukumura D, Gralla O et al (2004) Creation of long-lasting blood vessels. Nature 428(6979):138–139. https://doi.org/10.1038/428138a
3. Furth ME, Atala A, Van Dyke ME (2007) Smart biomaterials design for tissue engineering and regenerative medicine. Biomaterials 28(34):5068–5073. https://doi.org/10.1016/j.biomaterials.2007.07.042
4. Collier JH, Camp JP, Hudson TW et al (2000) Synthesis and characterization of polypyrrole-hyaluronic acid composite biomaterials for tissue engineering applications. J Biomed Mater Res 50(4):574–584. https://doi.org/10.1002/(SICI)1097-4636(20000615)50:4<574::AID-JBM13>3.0.CO;2-I
5. Schmidt CE, Baier JM (2000) Acellular vascular tissues: natural biomaterials for tissue repair and tissue engineering. Biomaterials 21(22):2215–2231. https://doi.org/10.1016/S0142-9612(00)00148-4
6. Kort-Mascort J, Flores-Torres S, Peza-Chavez O et al (2022) Decellularized ECM hydrogels: prior use considerations, applications, and opportunities in tissue engineering and biofabrication. Biomater Sci 11(2):400–431. https://doi.org/10.1039/d2bm01273a
7. Busch SM, Lorenzana Z, Ryan AL (2021) Implications for extracellular matrix interactions with human lung basal stem cells in lung development, disease, and airway modeling. Front Pharmacol 12:645858. https://doi.org/10.3389/fphar.2021.645858
8. Zhang Q, Hu, YX, Long X et al (2022) Preparation and application of decellularized ECM-based biological scaffolds for articular cartilage repair: a review. Front Bioeng Biotechnol 10:908082. https://doi.org/10.3389/fbioe.2022.908082
9. Poornima K, Francis AP, Hoda M et al (2022) Implications of three-dimensional cell culture in cancer therapeutic research.

Front Oncol 12:891673.
https://doi.org/10.3389/fonc.2022.891673
10. Gilbert TW, Sellaro TL, Badylak SF (2006) Decellularization of tissues and organs. Biomaterials 27(19):3675–3683.
https://doi.org/10.1016/j.biomaterials.2006.02.014
11. Schaner PJ, Martin ND, Tulenko TN et al (2004) Decellularized vein as a potential scaffold for vascular tissue engineering. J Vasc Surg 40(1):146–153.
https://doi.org/10.1016/j.jvs.2004.03.033
12. Brown BN, Badylak SF (2014) Extracellular matrix as an inductive scaffold for functional tissue reconstruction. Transl Res 163(4):268–285.
https://doi.org/10.1016/j.trsl.2013.11.003
13. Garreta E, Oria R, Tarantino C et al (2017) Tissue engineering by decellularization and 3D bioprinting. Mater Today 20(4):166–178.
https://doi.org/10.1016/j.mattod.2016.12.005
14. Kim BS, Choi JS, Kim JD et al (2012) Recellularization of decellularized human adipose-tissue-derived extracellular matrix sheets with other human cell types. Cell Tissue Res 348(3):559–567.
https://doi.org/10.1007/s00441-012-1391-y
15. Singelyn JM, DeQuach JA, Seif-Naraghi SB et al (2009) Naturally derived myocardial matrix as an injectable scaffold for cardiac tissue engineering. Biomaterials 30(29):5409–5416.
https://doi.org/10.1016/j.biomaterials.2009.06.045
16. Singelyn JM, Christman KL (2010) Injectable materials for the treatment of myocardial infarction and heart failure: the promise of decellularized matrices. J Cardiovasc Transl Res 3(5):478–486.
https://doi.org/10.1007/s12265-010-9202-x
17. Young DA, Ibrahim DO, Hu D et al (2011) Injectable hydrogel scaffold from decellularized human lipoaspirate. Acta Biomater 7(3):1040–1049.
https://doi.org/10.1016/j.actbio.2010.09.035
18. Seif-Naraghi SB, Horn D, Schup-Magoffin PJ et al (2012) Injectable extracellular matrix derived hydrogel provides a platform for enhanced retention and delivery of a heparin-binding growth factor. Acta Biomater 8(10):3695–3703.
https://doi.org/10.1016/j.actbio.2012.06.030
19. Gudapati H, Dey M, Ozbolat I (2016) A comprehensive review on droplet-based bioprinting: past, present and future. Biomaterials 102:20–42.
https://doi.org/10.1016/j.biomaterials.2016.06.012
20. Pati F, Song TH, Rijal G et al (2015) Ornamenting 3D printed scaffolds with cell-laid extracellular matrix for bone tissue regeneration. Biomaterials 37:230–241.
https://doi.org/10.1016/j.biomaterials.2014.10.012
21. Kim BS, Das S, Jang J et al (2020) Decellularized extracellular matrix-based bioinks for engineering tissue- and organ-specific microenvironments. Chem Rev 120(19):10608–10661.
https://doi.org/10.1021/acs.chemrev.9b00808
22. Sharifi R, Yang Y, Adibnia Y et al (2019) Finding an optimal corneal xenograft using comparative analysis of corneal matrix proteins across species. Sci Rep 9(1):1876.
https://doi.org/10.1038/s41598-018-38342-4
23. Oh JY, Kim MK, Lee HJ et al (2009) Processing porcine cornea for biomedical applications. Tissue Eng Part C Methods 15(4):635–645.
https://doi.org/10.1089/ten.tec.2009.0022
24. Du LQ, Wu XY, Pang KP et al (2011) Histological evaluation and biomechanical characterisation of an acellular porcine cornea scaffold. Br J Ophthalmol 95(3):410–414.
https://doi.org/10.1136/bjo.2008.142539
25. Aamodt JM, Grainger DW (2016) Extracellular matrix-based biomaterial scaffolds and the host response. Biomaterials 86:68–82.
https://doi.org/10.1016/j.biomaterials.2016.02.003
26. Crapo PM, Gilbert TW, Badylak SF (2011) An overview of tissue and whole organ decellularization processes. Biomaterials 32(12):3233–3243.
https://doi.org/10.1016/j.biomaterials.2011.01.057
27. Badylak SF, Gilbert TW (2008) Immune response to biologic scaffold materials. Semin Immunol 20(2):109–116.
https://doi.org/10.1016/j.smim.2007.11.003
28. Nagata S, Hanayama R, Kawane K (2020) Autoimmunity and the clearance of dead cells. Cell 140(5):619–630.
https://doi.org/10.1016/j.cell.2010.02.014
29. Zheng MH, Chen J, Kirilak Y et al (2005) Porcine small intestine submucosa (SIS) is not an acellular collagenous matrix and contains porcine DNA: possible implications in human implantation. J Biomed Mater Res Part B Appl Biomater 73B(1)1:61–67.
https://doi.org/1002/jbm.b.30170
30. Das S, Gao G, Lee JY et al (2019) Decellularized tissue matrix-based 3D tissue modeling. In: Cho DW (Ed.), Biofabrication and 3D Tissue Modeling. The Royal Society of Chemistry, UK, p.148–170.
https://doi.org/10.1039/9781788012683-00148
31. Arenas-Herrera JE, Ko IK, Atala A et al (2013) Decellularization for whole organ bioengineering. Biomed Mater 8(1):014106.
https://doi.org/10.1088/1748-6041/8/1/014106
32. Hoshiba T, Lu HX, Kawazoe N et al (2010) Decellularized matrices for tissue engineering. Expert Opin Biol Ther 10(12):1717–1728.
https://doi.org/10.1517/14712598.2010.534079
33. Keane TJ, Swinehart IT, Badylak SF (2015) Methods of tissue decellularization used for preparation of biologic scaffolds and in vivo relevance. Methods 84:25–34.
https://doi.org/10.1016/j.ymeth.2015.03.005
34. Kajbafzadeh AM, Javan-Farazmand N, Monajemzadeh M et al (2013) Determining the optimal decellularization and sterilization protocol for preparing a tissue scaffold of a human-sized liver tissue. Tissue Eng Part C Methods 19(8):642–651.
https://doi.org/10.1089/ten.tec.2012.0334
35. Zhou JY, Fritze O, Schleicher M et al (2010) Impact of heart valve decellularization on 3-D ultrastructure, immunogenicity and thrombogenicity. Biomaterials 31(9):2549–2554.
https://doi.org/10.1016/j.biomaterials.2009.11.088
36. Jiang WC, Cheng YH, Yen MH et al (2014) Cryo-chemical decellularization of the whole liver for mesenchymal stem cells-based functional hepatic tissue engineering. Biomaterials 35(11):3607–3617.
https://doi.org/10.1016/j.biomaterials.2014.01.024
37. Gratzer PF, Harrison RD, Woods T (2006) Matrix alteration and not residual sodium dodecyl sulfate cytotoxicity affects the cellular repopulation of a decellularized matrix. Tissue Eng 12(10):2975–2983.
https://doi.org/10.1089/ten.2006.12.2975
38. Heath DE (2019) A review of decellularized extracellular matrix biomaterials for regenerative engineering applications. Regen Eng Transl Med 5(2):155–166.
https://doi.org/10.1007/s40883-018-0080-0
39. Kabirian F, Mozafari M (2020) Decellularized ECM-derived bioinks: prospects for the future. Methods 171:108–118.
https://doi.org/10.1016/j.ymeth.2019.04.019
40. Hung SH, Su CH, Lee FP et al (2013) Larynx decellularization: combining freeze-drying and sonication as an effective method. J Voice 27(3):289–294.

https://doi.org/10.1016/j.jvoice.2013.01.018
41. Ahearne M, Coyle A (2016) Application of UVA-riboflavin crosslinking to enhance the mechanical properties of extracellular matrix derived hydrogels. J Mech Behav Biomed Mater 54:259–267. https://doi.org/10.1016/j.jmbbm.2015.09.035
42. Krumdieck CL, dos Santos J, Ho KJ (1980) A new instrument for the rapid preparation of tissue slices. Anal Biochem 104(1): 118–123. https://doi.org/10.1016/0003-2697(80)90284-5
43. Majorova D, Atkins E, Martineau H et al (2021) Use of precision-cut tissue slices as a translational model to study host-pathogen interaction. Front Vet Sci 8:686088. https://doi.org/10.3389/fvets.2021.686088
44. Smith PF, Gandolfi AJ, Krumdieck CL et al (1985) Dynamic organ culture of precision liver slices for toxicology. Life Sci 36(14):1367–1375. https://doi.org/10.1016/0024-3205(85)90042-6
45. Harris RJ, McMillan DB (2018) An Atlas of Comparative Vertebrate Histology. Elsevier, London, UK. https://doi.org/10.1016/C2012-0-06909-8
46. Levin L, Nilsson S, Hoeve J (2011) Adler's Physiology of the Eye. Elsevier Inc., St. Louis, Missouri, USA
47. Crespo-Moral M, García-Posadas L, López-García A et al (2020) Histological and immunohistochemical characterization of the porcine ocular surface. PLoS ONE 15(1):e0227732. https://doi.org/10.1371/journal.pone.0227732
48. Shamoto E, Altıntas Y (1999) Prediction of shear angle in oblique cutting with maximum shear stress and minimum energy principles. J Manuf Sci Eng 121(3):399–407. https://doi.org/10.1115/1.2832695
49. Behrens A, Langenbucher A, Kus MM et al (2000) Experimental evaluation of two current-generation automated microkeratomes: the Hansatome and the Supratome. Am J Ophthalmol 129(1):59–67. https://doi.org/10.1016/S0002-9394(99)00269-X
50. Feather Safety Razor Co., Ltd. (2023) Surgery. https://www.feather.co.jp/en/pdf/m_Products/surgery2112.pdf
51. Ziegler JG, Nichols NB (1942) Optimum settings for automatic controllers. J Fluids Eng 64(8):759–765. https://doi.org/10.1115/1.4019264
52. McCormack AS, Godfrey KR (1998) Rule-based autotuning based on frequency domain identification. IEEE Trans Contr Syst Technol 6(1):43–61. https://doi.org/10.1109/87.654876